DOI: 10.13009/EUCASS2023-475
Aerospace Europe Conference 2023 – 10TH EUCASS – 9TH CEAS

Load Flow Analysis of Hybrid AC-DC Power Systems for the Application in Electrified Aircraft Propulsion

Victor Bahrs[⋆†]*, Jonas Ludowicy*[⋆]*, Martin Staggat*[⋆] *and Stefanie de Graaf*[⋆]
[⋆]*German Aerospace Center (DLR), Institute of Electrified Aero Engines,*
Department: Architecture of Propulsion System,
Lieberoser Str. 13a, 03046 Cottbus, Germany
victor.bahrs@dlr.de
[†]Corresponding author

Abstract

To reduce the emissions of aviation the electrification of aircraft propulsion is of particular research interest. Here, the power provided to the electric propulsors is distributed within the powertrain either in form of direct or alternating current. Therefore, an implementation of power flow simulation is presented, which can be used in aircraft powertrain sizing. The methodology enables bidirectional power flow and adds the possibility to change the voltage level between buses within the system. Furthermore, the proposed methodology accounts for functional dependencies of system parameters, like the converter efficiency on the power flow. The methodology is validated and exemplary applied on an electrified propulsion system topology.

Nomenclature

Symbols

η	Efficiency	[%/100]
ψ	Admittance phase angle	[deg]
θ	Voltage phase angle	[deg]
θ_c	AC-AC converter phase shift	[deg]
φ	AC-DC converter phase shift	[deg]
B	Susceptance of an AC line	[S]
C	Boolean matrix of converter existence	[−]
CAt	Boolean matrix of converter placement	[−]
D	Boolean matrix of line type	[−]
G	Conductance of an AC or DC line	[S]
I	Current	[A]
i	Imaginary number	[−]
M	Modulation index AC-DC converter	[−]
N	Number of buses in a system	[−]
P	Active power	[W]
Q	Reactive power	[VAr]
R	Resistance of an AC or DC line	[Ω]
t	Voltage ratio AC-AC & DC-DC converter	[−]
U	Boolean matrix of bus connection	[−]
V	Voltage	[V]
W	Boolean vector of bus type	[−]
X	Reactance of an AC line	[Ω]
Y	Admittance of an AC or DC line	[S]
Z	Impedance of an AC or DC line	[Ω]

Indices

AC	Alternating current
C	Converter
DC	Direct current
G	Generator
I	Inverter
L	Load
nm	Bus number indices
pu	Per-unit
R	Rectifier
rms	Root-mean square
tmp	Temporary

DOI: 10.13009/EUCASS2023-475

1. Introduction

In order to limit global warming, ambitious political goals have been formulated. The "Flightpath 2050" resolution summarizes the targets set by the Advisory Committee of aviation research and innovation in Europe (ACARE). To achieve these ambitious goals, i.e. reduction of nitrogen oxides by 90 % and carbon dioxide emissions by 75 % by 2050, innovations in the area of aircraft propulsion systems have to be achieved [1]. Electrification of aero engines is one possible approach for reducing greenhouse gas emissions in aviation. Therefore, many different powertrain topologies can be considered. Batteries, fuel cells or even gas turbines coupled to a generator can supply the powertrain with electric power, which then can be transformed to mechanical power by electric motors. Furthermore, all the mentioned power suppliers can also be combined in parallel or series hybrid topologies. If electrical power from renewable sources is used for storage in a battery or for the production of fuel, like hydrogen or sustainable aviation fuel (SAF), an emission free aircraft is possible. To size the components of such a powertrain and to assess potential new topologies, the electric power flow distribution has to be modelled. These novel aircraft propulsion systems contain both alternating current (AC) and direct current (DC). This is due to the fact that sources, such as fuel cells and batteries provide DC, while the electrical motors are typically fed by AC. Nevertheless, depending on the topology and voltage level, both DC and AC systems can be used for power distribution from the sources to the consumers. To analyse the load flow throughout the whole powertrain, a suitable methodology for hybrid AC-DC systems is necessary. Furthermore, the methodology has to provide bidirectional load flow in the electric system to enable, for instance, the recharging of batteries during descent. In addition, the power flow simulation should not be computationally intensive, while still achieving sufficient accuracy.
Different approaches can be found in the literature. In electric powertrain simulations in the automotive area mainly Matlab/Simulink is used [2–4], which is also used for some aircraft applications [5]. However, the coupling of electric components in aircraft powertrain simulation often is achieved by a direct transfer of electric current and voltage [6–9]. By transferring current, voltage and phase angle directly from one component to another, the power flow direction has to be defined and the bidirectionality may be lost. In order to avoid a predefinition of the power flow direction the present paper introduces a different approach for electric powertrain analysis.
Electric load flow analysis has been used for a long time to analyse and optimise the power flow in electrical energy supply grids [10]. Although initially power grids mainly consist of only AC power, hybrid AC-DC systems are in the focus of research in energy supply as well. Different approaches were introduced for adapting load flow analysis for hybrid systems [11–13]. Ahmed *et al.* [11] generalise the load flow analysis for hybrid AC-DC distribution systems, which allows to solve the DC and AC part of the system simultaneously and also enables bidirectional power flow between those parts. This concept is the basis for the methodology presented in this paper. It is modified and extended to be applicable to electric powertrains for aircraft propulsion. Besides some modifications of the published methodology, mainly converters for voltage level changes and consideration of functionally interdependent parameters are added. The methodology is extensively described, validated and exemplary applied for an electrified aircraft powertrain sizing.

2. Methodology

Load flow analysis provides a methodology for analysing the power flow in electric distribution systems. The method uses a system of buses with voltage and phase angle properties, and connections with impedance values connecting them. By balancing active and reactive power at the buses with Ohm's and Kirchhoff's law the power flow can be calculated and the system solved [14]. The complex impedance $\underline{Z}$ of an AC connection between buses is defined by

$$\underline{Z} = R + iX \quad , \tag{1}$$

where the real part R is the resistance and the imaginary part X is the reactance. The impedance values for each connection between bus n and m constitute the impedance matrix $\underline{Z}_{nm}$ for the electrical system. For load flow analysis the impedance matrix is transformed to the corresponding admittance matrix $\underline{Y}_{nm}$. The admittance matrix needs to be calculated by definition [15] for the main diagonal elements

$$\text{for } m = n: \quad \underline{Y}_{nn} = \frac{1}{\underline{Z}_{n0}} + \sum_{m}^{N} \frac{1}{\underline{Z}_{nm}} \tag{2}$$

and for the non diagonal elements

$$\text{for } m \neq n: \quad \underline{Y}_{nm} = \underline{Y}_{mn} = -\frac{1}{\underline{Z}_{nm}} \tag{3}$$

separately, where $\underline{Z}_{n0}$ is the grounding impedance at bus n and N is the total number of buses in the system.

DOI: 10.13009/EUCASS2023-475

The admittance matrix is then used for the calculation of active (P) and reactive power (Q) flows towards any bus n

$$\frac{P_n - iQ_n}{\underline{\hat{V}}_n} = \sum_m^N (\underline{Y}_{nm} \cdot \underline{V}_m) \quad , \tag{4}$$

where $\underline{V}$ and $\underline{\hat{V}}$ are the complex and complex conjugated bus voltage respectively [16].
The complex bus voltage can also be described in its polar form

$$\underline{V}_n = V_n \cdot e^{i\theta_n} \quad , \tag{5}$$

where θ and V are the voltage phase angle and magnitude respectively. The admittance is defined by the conductance G and susceptance B as

$$\underline{Y} = G + iB \quad . \tag{6}$$

With the definitions of Equations (5) and (6), Equation (4) can be split in real and imaginary parts to calculate P_n and Q_n at each bus n through

$$P_n = V_n \sum_m^N V_m (G_{nm} \cos(\theta_n - \theta_m) + B_{nm} \sin(\theta_n - \theta_m)) \tag{7}$$

$$Q_n = V_n \sum_m^N V_m (G_{nm} \sin(\theta_n - \theta_m) - B_{nm} \cos(\theta_n - \theta_m)) \quad . \tag{8}$$

With the calculated active and reactive power from Equations (7) and (8) a balance with injected power values, i.e. load and generator power, is possible at each bus. By taking the difference between calculated and injected power values, a function F is determined:

$$F(\vec{x}) = \begin{cases} P_{inj} - P_{cal} \\ Q_{inj} - Q_{cal} \end{cases} \quad . \tag{9}$$

The function itself is dependent on the electric parameters of the system combined in $\vec{x}$, like voltage phase angles and magnitudes, admittance values, and injected powers. A solution of the load flow in the electric system can be found by minimising the function F. Therefore the objective is

$$\min ||F(\vec{x})||_2 = 0 \quad . \tag{10}$$

The number of unknown parameters has to match the number of Equations in the function F, whereby each bus has to fit to one of the types listed in Table 1.

Table 1: AC bus types [15]

Bus type	**Known**	**Unknown**
Slack bus	V, θ	P_{inj}, Q_{inj}
P-Q (load) bus	P_{inj}, Q_{inj}	V, θ
P-V (generator) bus	P_{inj}, V	Q_{inj}, θ

The described approach is widely used for analysing the load flow in electric distribution systems. However, what has been described up until this point is only applicable to AC distribution systems. The concept of minimising the difference between the calculated power and the injected power, can be used for DC and hybrid AC-DC systems as well. To be able to apply this approach to such systems, the calculation of the power flow through connections has to be adapted. For DC power systems no imaginary parts exist, like reactive power or reactance, which leads to a simplified power calculation of

$$P_n = V_n \sum_m^N V_m G_{nm} \tag{11}$$

analogous to Equation (7) and a modified set of bus types as presented in Table 2.

DOI: 10.13009/EUCASS2023-475

Table 2: DC bus types [11]

Bus type	Known	Unknown
P (load) bus	P_{inj}	V
V (generator / slack) bus	V	P_{inj}

Following the load flow theory of AC and DC systems, the bidirectional connection of these systems has to be analysed. A generalised approach to the load flow analysis of AC-DC hybrid distribution systems was published by Ahmed *et al.* [11]. Here, an AC-DC converter model was introduced to connect voltage levels on DC and AC side and enable load flow calculation across the converter. The AC and DC voltage levels are linked by a modulation index M defined by

$$V_n^{AC} = M \cdot V_{tmp}^{DC} \quad , \tag{12}$$

where V_n^{AC} and V_{tmp}^{DC} represent the effective AC and DC voltages directly before and after the converter as depicted in Figure 1. Based on the type of the inverter or rectifier the maximum modulation index is limited. For a three level neutral point clamped (3L-NPC) inverter it is for example $M_{max} = 0.707$ [17]. Generally, this value can be found in literature on the applied inverter topology.

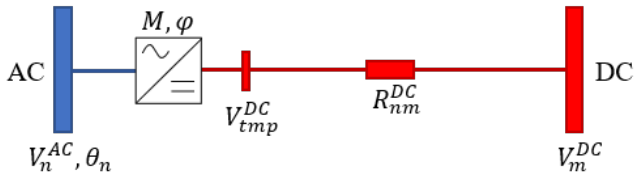

Figure 1: Two bus system with an AC-DC Converter

The active and reactive power flows across the converter are calculated as follows [11]:

$$\text{from } n \text{ to } m: \quad P_{nm} = G_{nm}^{DC} \cdot \left(M^{-2}(V_n^{AC})^2 - M^{-1} V_n^{AC} V_m^{DC}\right) \cdot \left(\frac{a_1}{\eta_{nm,r}} + b_1 \eta_{nm,i}\right) \tag{13}$$

$$Q_{nm} = P_{nm} \cdot \tan\varphi \tag{14}$$

$$\text{from } m \text{ to } n: \quad P_{mn} = G_{mn}^{DC} \cdot \left((V_m^{DC})^2 - M^{-1} V_n^{AC} V_m^{DC}\right) \tag{15}$$

$$Q_{mn} = P_{mn} \cdot \tan\varphi \quad . \tag{16}$$

The converter efficiency for rectifier and inverter mode are $\eta_{nm,r}$ and $\eta_{nm,i}$ respectively. To consider the direction of the power flow and therefore the currently active converter mode (inverting or rectifying), two parameters a_1 and b_1 are being introduced [11] as

$$\begin{aligned} a_1 &= 0.5 \cdot \left(1 + \text{sign}(M^{-1} V_n - V_m)\right) \\ b_1 &= 0.5 \cdot \left(1 - \text{sign}(M^{-1} V_n - V_m)\right) \end{aligned} \quad \text{, where } \text{sign}(x) = \begin{cases} 1 & , x > 0 \\ -1 & , x < 0 \\ 0 & , x = 0 \end{cases} \quad . \tag{17}$$

Dependent on the direction of the power flow either a_1 or b_1 ends up being equal to one while the other one is zero. With this approach, only one of the efficiencies is taken into account. The published methodology is extended in the following by DC-DC and AC-AC converters. The converters are modelled analogous to the AC-DC converter, to be consistent with the generalised load flow analysis.

As shown in Figure 2 a DC-DC converter can be used to change the voltage level between two DC buses. The voltage ratio t is defined as

$$t = \frac{V_n^{DC}}{V_{tmp}^{DC}} \quad , \tag{18}$$

while the power flow across the converter is specified through

DOI: 10.13009/EUCASS2023-475

$$\text{from } n \text{ to } m: \quad P_{nm} = G_{nm}^{DC} \cdot \left(t^{-2}(V_n^{DC})^2 - t^{-1} V_n^{DC} V_m^{DC}\right) \cdot \left(\frac{a_2}{\eta_{nm,1}} + b_2 \eta_{nm,2}\right) \tag{19}$$

$$\text{from } m \text{ to } n: \quad P_{mn} = G_{mn}^{DC} \cdot \left((V_m^{DC})^2 - t^{-1} V_n^{DC} V_m^{DC}\right) \quad , \tag{20}$$

where $\eta_{nm,1}$ and $\eta_{nm,2}$ describe the efficiencies for the two modes of boost and buck conversion, depending on the defined voltage ratio t. The parameters a_2 and b_2 are defined as

$$\begin{aligned} a_2 &= 0.5 \cdot \left(1 + \text{sign}(t^{-1} V_n - V_m)\right) \\ b_2 &= 0.5 \cdot \left(1 - \text{sign}(t^{-1} V_n - V_m)\right) \end{aligned} \tag{21}$$

and determine which one of the efficiency terms in Equation (19) will disappear.

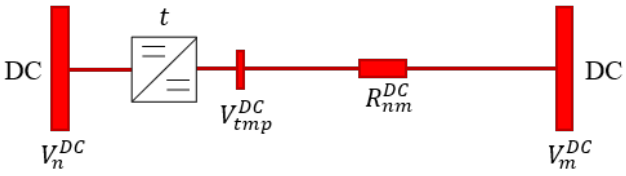

Figure 2: Two bus system with a DC-DC Converter

The AC-AC converter modelling is nearly equivalent to the DC-DC converter implementation, except for the complex values needed in the AC case. A simple two bus system with an AC-AC converter is shown in Figure 3.

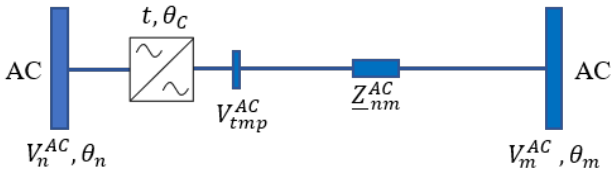

Figure 3: Two bus system with an AC-AC Converter

Because of the AC power, the converter has both a voltage ratio magnitude t and a phase shift θ_c. The complex voltage ratio $\underline{t}$ is defined as

$$\underline{t} = t \cdot e^{i\theta_c} \quad , \quad \text{with} \quad t = \frac{V_n^{AC}}{V_{tmp}^{AC}} \quad . \tag{22}$$

The power flow across the AC-AC converter has a reactive power part and is therefore defined in forward direction as

$$\text{from } n \text{ to } m: \quad P_{nm} = \left(G_{nm}^{AC} t^{-2} (V_n^{AC})^2 - t^{-1} V_n^{AC} V_m^{AC} Y_{nm} \cos(\theta_n - \theta_m - \psi_{nm} + \theta_c)\right) \cdot \left(\frac{a_2}{\eta_{nm,1}} + b_2 \eta_{nm,2}\right) \tag{23}$$

$$Q_{nm} = -B_{nm}^{AC} t^{-2} (V_n^{AC})^2 - t^{-1} V_n^{AC} V_m^{AC} Y_{nm} \sin(\theta_n - \theta_m - \psi_{nm} + \theta_c) \tag{24}$$

and in reverse direction by

$$\text{from } m \text{ to } n: \quad P_{mn} = G_{mn}^{AC} (V_m^{AC})^2 - t^{-1} V_n^{AC} V_m^{AC} Y_{mn} \cos(\theta_n - \theta_m - \psi_{nm} - \theta_c) \tag{25}$$

$$Q_{mn} = -B_{mn}^{AC} (V_m^{AC})^2 - t^{-1} V_n^{AC} V_m^{AC} Y_{mn} \sin(\theta_n - \theta_m - \psi_{mn} - \theta_c) \quad . \tag{26}$$

The admittance of the connection $\underline{Y}_{nm}$ is thereby defined by its magnitude Y_{nm} and phase angle ψ_{nm}

$$\underline{Y}_{nm} = Y_{nm} \cdot e^{i\psi_{nm}} \quad . \tag{27}$$

DOI: 10.13009/EUCASS2023-475

To calculate the power at a bus, all the connected power flows from Equations (7), (8) (11), (13) - (16), (19) - (20), (23) - (26) must be considered. In order to generalise the calculation Ahmed *et al.* [11] defined a system of matrices to activate and deactivate the load flow parts according to the type of the connection present. For the added DC-DC and AC-AC converter additional system matrices are defined and listed in the Nomenclature and in the Appendix (Table 9). A complete set of Equations for the active and reactive power flows at one bus can also be found in the Appendix in Equations (32) - (35).
When power distribution systems are evaluated where converters set significant voltage ratios, a coupling of different per-unit (pu) systems may be necessary. The pu systems must be defined for closed parts of the power distribution system and have to be coupled by the introduced converters. Therefore, one has to adapt the modulation indices and voltage ratio values for the converters according to the varying pu systems. For this, the introduced converter indices from Equations (12), (18) and (22) have to be multiplied by the base voltage ratio of the appropriate pu systems, i.e. of buses n and m. Exemplary adapting the AC-DC converter index for the two bus system shown in Figure 1 leads to

$$M_{pu} = \frac{V_n^{AC}}{V_{tmp}^{DC}} \cdot \frac{V_{base,n}^{AC}}{V_{base,m}^{DC}} \quad , \tag{28}$$

while the appropriate per-unit DC-DC converter voltage ratio for the system shown in Figure 2 calculates to

$$t_{pu} = \frac{V_n^{DC}}{V_{tmp}^{DC}} \cdot \frac{V_{base,n}^{DC}}{V_{base,m}^{DC}} \quad . \tag{29}$$

Furthermore, the option to define parameters as functionally dependent on others is implemented. An inner iteration is used to recalculate certain parameters, such as the efficiency of an inverter based on the bus voltage, the modulation index or the power flow. The iteration logic for both the load flow and recalculation iteration is shown in Figure 4. The load flow is iterated according to the definition in Equation (10), while the functional dependent parameters are iterated until they have no changes from the last time step. Therefore, ϵ is used as converge criterion with a precision of 10^{-6}.

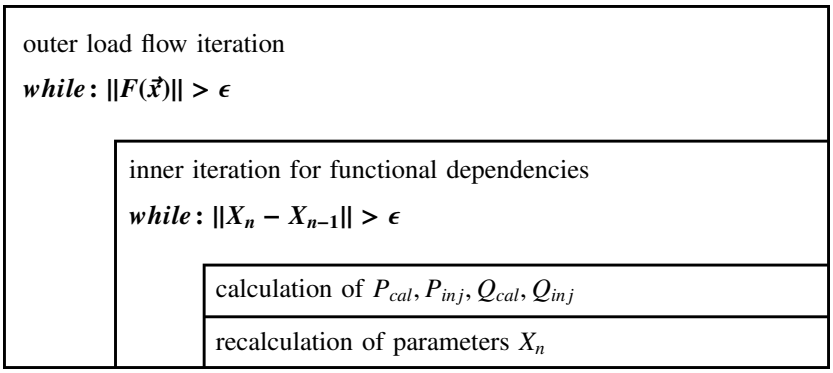

Figure 4: Iteration logic for additional parameters with functional dependencies

With this additional iteration the load flow methodology can be used in the sizing process of electrified aircraft powertrains. Component models for converters or motors can be coupled with the load flow algorithm via the functional dependencies. Based on the power flows, voltage levels or phase angles calculated using this method, all components can be sized regarding mass, volume and efficiency. The efficiency can be determined iteratively in the load flow analysis by enabling the coupling of the power flow distribution and component properties calculation. Furthermore, off-design studies with already sized components can be performed. Parameters that are still dependent on the power flow distribution, like the efficiency of a converter, are recalculated and iterated as shown in Figure 4.

3. Results

In the following, the developed method for load flow calculation is validated against various examples from literature and the commercial software NEPLAN [18]. After validation, the presented method is applied to an exemplary electrical architecture representing a distributed electric propulsion system for a regional-size aircraft. The results are presented in Section 3.2 accordingly.

DOI: 10.13009/EUCASS2023-475

3.1 Validation of load flow analysis method

Figure 5 depicts a modified IEEE 33 bus system published by Ahmed *et al.* [11]. The DC and AC line impedances as well as all load and generator (Gen) data are also extracted from this work. Furthermore, the same per-unit base values are used, namely $V_{base}^{AC} = 12.66\,\text{kV}$ and $V_{base}^{DC} = 20.67\,\text{kV}$. The efficiency of all converters is set to $\eta = 0.95$ and all power factors are assumed to be $\cos(\varphi) = 0.95$.

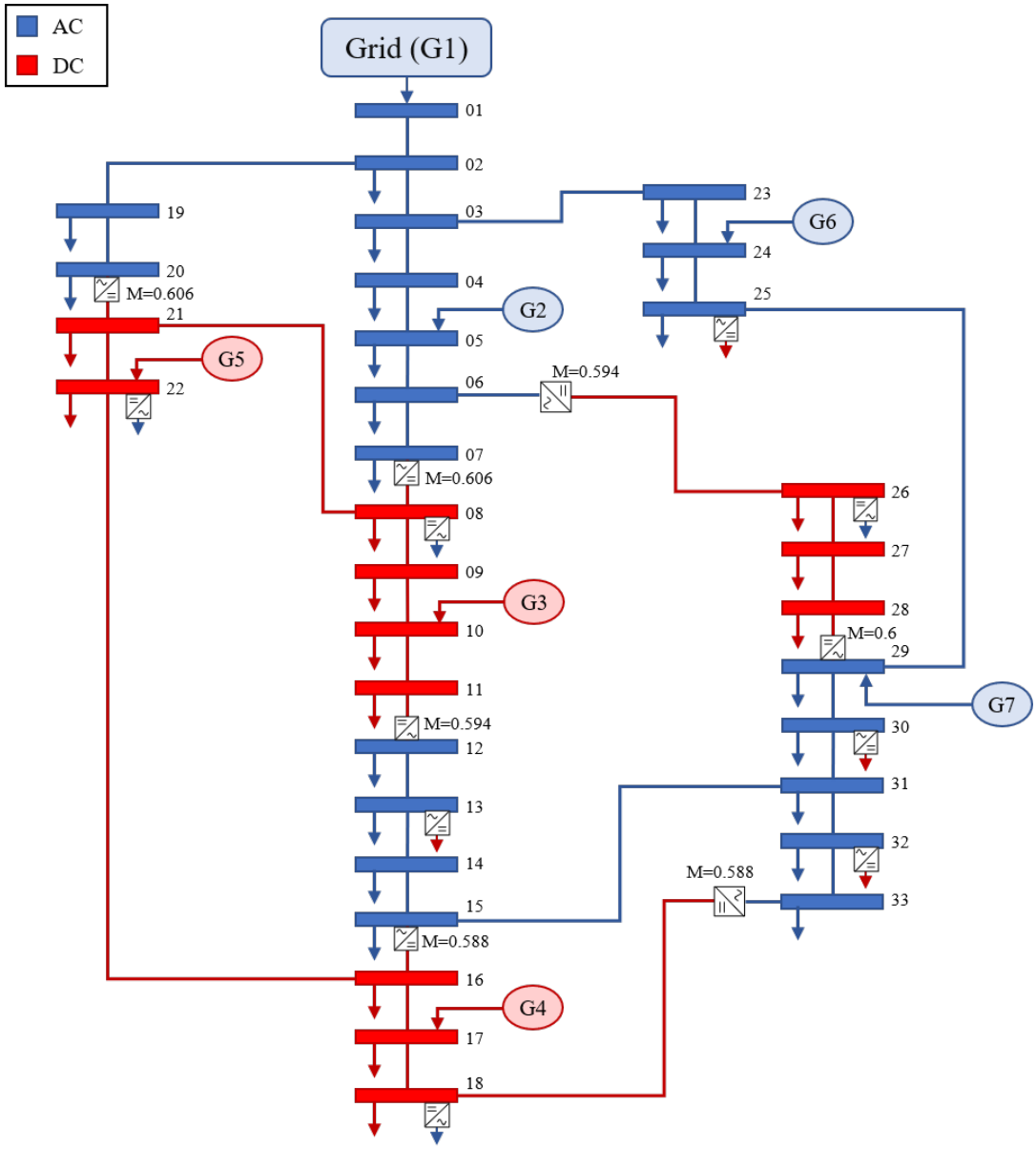

Figure 5: Modified IEEE 33 bus system adapted from [11]

The results of the described load flow (LF) method match the published results with a maximum relative error of 0.036 %, as listed in detail in Table 3. The differences are assumed to be caused by rounding and machine precision and are therefore acceptable for validation purposes.

Figure 6 illustrates an AC system with four buses and an AC-AC converter between bus 1 and 2. This system is used to validate the additionally implemented AC-AC converter.

DOI: 10.13009/EUCASS2023-475

Table 3: Results of the 33 bus system compared to Ahmed *et al.* [11]

	LF Model Results		**Ahmed *et al.* [11]**			**LF Model Results**		**Ahmed *et al.* [11]**	
Bus no. (type)	Voltage (p.u.)	θ (deg.)	Voltage (p.u.)	θ (deg.)	**Bus no. (type)**	Voltage (p.u.)	θ (deg.)	Voltage (p.u.)	θ (deg.)
1 (AC)	1.05000	0.00000	1.05000	0.00000	18 (DC)	1.03930	-	1.03930	-
2 (AC)	1.04709	−0.00972	1.04709	−0.00972	19 (AC)	1.04503	−0.05930	1.04503	−0.05930
3 (AC)	1.03776	−0.02780	1.03776	−0.02781	20 (AC)	1.02871	−0.43951	1.02871	−0.43950
4 (AC)	1.03360	−0.03683	1.03360	−0.03683	21 (DC)	1.03702	-	1.03702	-
5 (AC)	1.03000	−0.05113	1.03000	−0.05114	22 (DC)	1.03715	-	1.03715	-
6 (AC)	1.01912	−0.27694	1.01912	−0.27694	23 (AC)	1.03477	−0.05338	1.03477	−0.05338
7 (AC)	1.01869	−0.29890	1.01869	−0.29890	24 (AC)	1.03000	−0.11852	1.03000	−0.11852
8 (DC)	1.02923	-	1.02923	-	25 (AC)	1.02238	−0.21869	1.02238	−0.21870
9 (DC)	1.02674	-	1.02674	-	26 (DC)	1.04951	-	1.04951	-
10 (DC)	1.02479	-	1.02479	-	27 (DC)	1.04808	-	1.04808	-
11 (DC)	1.02430	-	1.02430	-	28 (DC)	1.04371	-	1.04371	-
12 (AC)	0.99317	−0.62316	0.99317	−0.62317	29 (AC)	1.02000	−0.22491	1.02000	−0.22492
13 (AC)	0.99215	−0.66567	0.99215	−0.66568	30 (AC)	1.01404	−0.24913	1.01404	−0.24914
14 (AC)	0.99224	−0.66362	0.99225	−0.66363	31 (AC)	1.00228	−0.50557	1.00228	−0.50558
15 (AC)	0.99449	−0.62943	0.99449	−0.62944	32 (AC)	1.00006	−0.57216	1.00006	−0.57217
16 (DC)	1.03692	-	1.03692	-	33 (AC)	0.99823	−0.63484	0.99823	−0.63485
17 (DC)	1.03884	-	1.03884	-					
Gen no. (type)	P_G (kW)	Q_G (kVAr)	P_G (kW)	Q_G (kVAr)	**Gen no. (type)**	P_G (kW)	Q_G (kVAr)	P_G (kW)	Q_G (kVAr)
1 (AC)	4343.52	1889.99	4343.5	1890.0	6 (AC)	500	243.54	500	243.5
2 (AC)	500	139.99	500	140.00	7 (AC)	500	81.88	500	81.9

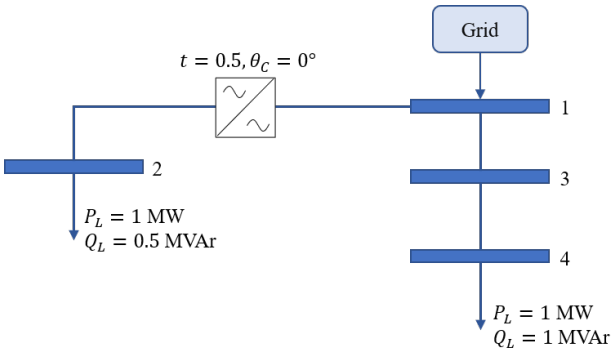

Figure 6: Four bus AC system

Table 4 lists the line impedance values of the analysed AC system. The AC-AC converter is initialised with a voltage ratio of $t = 0.5$ and a phase shift of $\theta_C = 0°$. For validation purposes, the system is simulated with the proposed LF model as well as with the commercial software NEPLAN [18]. As listed in Table 5, the results of the load flow analysis match the NEPLAN results with a maximum relative error of 0.02 %. With this, the implementation of the AC-AC converters can be considered as sufficiently validated for the purpose of its application.

Table 4: Impedance values for the four bus AC system

From bus	**Towards bus**	**Resistance (Ω)**	**Reactance (Ω)**
1	2	1.0	1.0
1	3	0.5	1.0
3	4	2.0	1.0

DOI: 10.13009/EUCASS2023-475

Table 5: Results of the four bus AC system simulation compared to NEPLAN

	LF Model Results		NEPLAN Results			LF Model Results		NEPLAN Results	
Bus no.	Voltage (kV)	θ (deg.)	Voltage (kV)	θ (deg.)	**Bus no.**	Voltage (kV)	θ (deg.)	Voltage (kV)	θ (deg.)
1	10	0	10	0	3	9.8430	-0.31029	9.8430	-0.31022
2	19.9247	-0.07189	19.9247	-0.07189	4	9.5275	0.30069	9.5276	0.30064
Gen	P_G (kW)	Q_G (kVAr)	P_G (kW)	Q_G (kVAr)					
Grid	2.05823	1.54721	2.05803	1.54710					

Finally, the DC load flow and the DC-DC converters are validated. Therefore, an electrical system presented by Wang *et al.* [19] was used, which is shown in Figure 7. The system consists of an AC grid connected by a rectifier to a DC system with 14 buses. Two more generators – one AC and one DC – and 12 DC loads are connected to the buses in this system. The system is split into two parts connected through DC-DC converters. The buses 1 to 5 are on a voltage level of 10 kV, while the remaining buses are on a level of 380 V. The converter voltage ratios are noted directly in Figure 7, where the converter between bus 5 and 6 is modelled with a constant output voltage of 380 V and consequently with a variable voltage ratio. All other required information, such as the line resistances, load and generator data, are the same as those of the aforementioned publication.

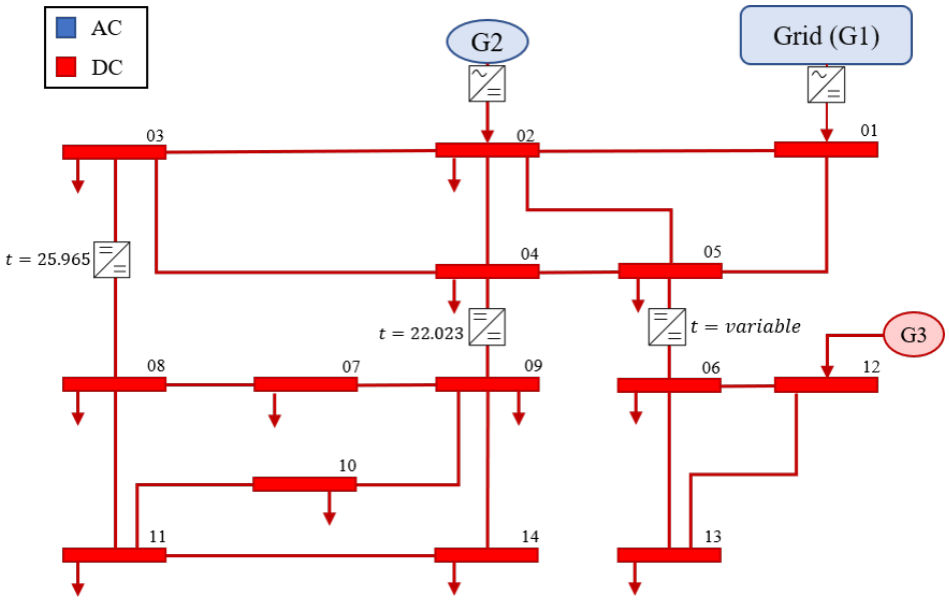

Figure 7: 14 bus DC system based on [19]

Table 6 presents a comparison of the calculated and published results of Wang *et al.* [19]. The bus voltages of the high voltage part (bus 1 to 5) match the published data without any error. For the low voltage section (bus 6 to 14) a maximum relative error of 0.0032 % was found. Consequently, the proposed load flow analysis is also considered sufficiently validated for the application of pure DC load flow and DC-DC converters.

3.2 Distributed electric propulsion study

In this section, the presented and validated load flow methodology is applied on an electric powertrain for aircraft application. In a first step, the aforementioned functional dependencies of system parameters are evaluated with the use of two simple two bus systems, which are depicted in Figure 8 and 9. Both systems are calculated firstly without any functional dependencies and secondly for the case of one functional dependent parameter. Thereby, the reliable functionality of this additional feature is proven. It is examined whether a solution for systems with functional dependent parameters can be found and whether the solution shows comprehensible results.

DOI: 10.13009/EUCASS2023-475

Table 6: Results of the 14 bus DC system compared to Wang *et al.* [19]

	Voltage (V)			Voltage (V)	
Bus no.	LF Model Results	Wang *et al.* [19]	**Bus no.**	LF Model Results	Wang *et al.* [19]
1	10000.000	10000.000	8	380.107	380.119
2	10000.000	10000.000	9	380.513	380.525
3	9930.469	9930.469	10	380.138	380.149
4	9911.962	9911.962	11	379.919	379.930
5	9953.105	9953.105	12	380.157	380.157
6	380.000	380.000	13	379.997	379.997
7	380.207	380.219	14	380.130	380.142

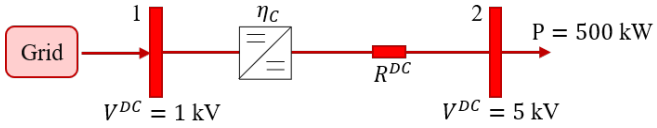

Figure 8: Two bus DC system with DC-DC converter

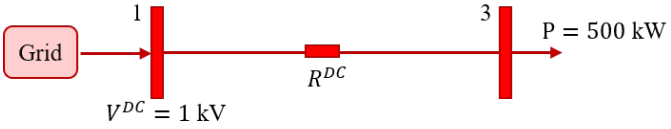

Figure 9: Two bus DC system

Firstly, the efficiency η_C of the DC-DC converter between bus 1 and 2 in Figure 8 is considered functionally dependent on the power flow P_{12}. The assumed dependency is given by

$$\eta_C = 1 - |P_{12} \cdot 10^{-7}| \quad . \tag{30}$$

The converter efficiency decreases with increasing power flow from bus 1 to bus 2. The system is initially calculated with a converter efficiency of $\eta_C = 1$ and then iterated with the dependency from Equation (30) and sizing logic of Figure 4 to converge. The results for the two calculations and the differences between them are documented in Table 7.

Table 7: Results for the two bus system with a DC-DC converter and variable converter efficiency

Parameter (unit)	**Bus no.**	**Fix efficiency**	**Variable efficiency**	**Difference**
η_C (%/100)	$1 \rightarrow 2$	1	0.947	−5.3 %
$P_{G,1}$ (kW)	1	501	528.98	+5.3 %
$P_{L,2}$ (kW)	2	500	500	-
t_{12} (-)	$1 \rightarrow 2$	0.1996	0.1996	-
V_1 (V)	1	1000	1000	-
V_2 (V)	2	5000	5000	-

Due to the power flow from bus 1 to bus 2 the converter efficiency decreases by 5.3 %. The same amount of power increase is consistently determined at the slack bus 1. In the case of fixed efficiency, only the power loss across the connection ($R_{12} = 0.1\,\Omega$) needs to be considered, which leads to a total power loss of about 1 kW. With the reduced converter efficiency the power loss increases to approximately 29 kW, which has to be provided by the slack generator in addition to the actual load power of 500 kW at bus 2.

It is even possible to vary the resistance of line connections between buses as functional dependent. To demonstrate this, the system shown in Figure 9 and the dependency on the current flow I_{13} is used through

$$R_{13}^{DC} = 0.02 + |I_{13} \cdot 10^{-5}| \quad . \tag{31}$$

DOI: 10.13009/EUCASS2023-475

Similar to the previous example of variable converter efficiency, the system is calculated initially for a state with fixed resistance followed by a calculation with variable resistance. The results for both calculations are listed in Table 8.

Table 8: Results for the two bus system with fixed and variable DC line resistance

Parameter (unit)	**Bus no.**	**Initial calculation**	**Variable efficiency**	**Difference**
R_{13}^{DC} (Ω)	$1 \rightarrow 3$	0.02	0.025	+20 %
$P_{G,1}$ (kW)	1	505.1	506.4	+0.26 %
$P_{L,3}$ (kW)	3	500	500	-
V_1 (V)	1	1000	1000	-
V_3 (V)	3	989.9	987.31	−0.26 %

Due to the power and current flow between bus 1 and 3, the resistance increases by 20 % in comparison to the initial setup. As a result of the rise in resistance, the losses increase as well and the slack power needs to be higher. In fact, the losses increase by approximately 25 % from 5.1 to 6.4 kW. Due to the higher power flow between buses 1 and 3, the relative increase of the losses is higher then the relative increase of the resistance. According to the higher losses, the slack power increases by 0.26 %. With higher resistance the voltage drop increases as well, which results in a load bus voltage reduction of 0.26 %. The slack bus voltage and the load power remain constant as expected.
In a next step the developed methodology was applied to the electrical architecture of an aircraft powertrain. This powertrain is to be sized for a regional aircraft with six electric propulsors as per Figure 10. This is a representative concept and follows the narrative of many electrified aero engine concepts currently being discussed and investigated in research: the distributed electric propulsion system.

Figure 10: Exemplary regional aircraft with six propulsion units

The example investigated here, consists of a propulsion system with a 12 bus electrical architecture, where a fuel cell operating at 1000 V and a battery stack operating at 500 V are used as power sources. This architecture is illustrated in Figure 11. Six AC loads, representing the electric machines, are connected by inverters to the DC powertrain distribution system. The two power sources are both connected by DC-DC converters to achieve a fixed voltage level of $V^{DC} = 2\,\text{kV}$ for power distribution. The inverters are modelled with a constant effective output AC voltage of $V_{rms}^{AC} = 1\,\text{kV}$. All lines up to bus 6 assume a resistance of $0.05\,\Omega$, while the lines connecting the buses 5 and 6 with the buses 7 to 12 assume $0.1\,\Omega$. Furthermore, the DC-DC converters and the inverters are modelled with an efficiency of 95 %, and the power factors of the inverters are set to 0.95. The fuel cell is assumed as a DC generator with a power supply between $0.3 - 2.7\,\text{MW}$. For the load flow analysis the fuel cell is operated at a constant generator power within this range, whereas the battery operates as buffer for the remaining power needed.
Figure 12 shows the results for an exemplary calculation. Here, an active power of $P = 600\,\text{kW}$ is assumed for each AC load, representing a high power demand flight phase like take-off. The thick arrows indicate the power flow direction and are labeled with the magnitude of the power flow. Due to the high power requested at this operating point, the fuel cell delivers its maximum power of 2.7 MW. Therefore, the battery needs to deliver an additional power of 1.515 MW.

DOI: 10.13009/EUCASS2023-475

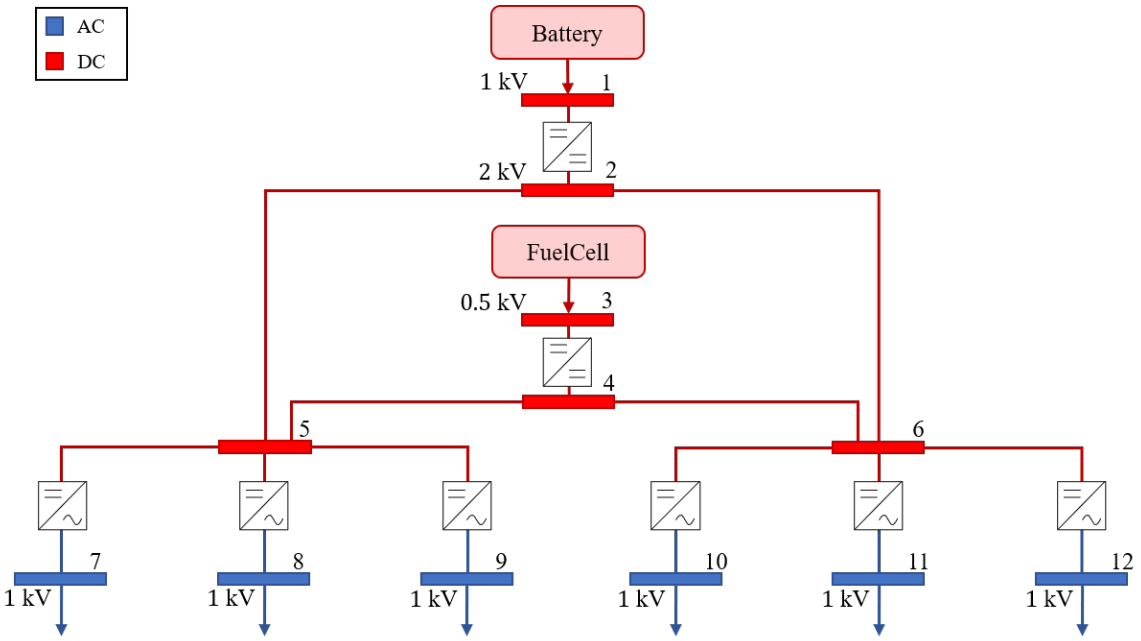

Figure 11: 12 bus powertrain for regional aircraft

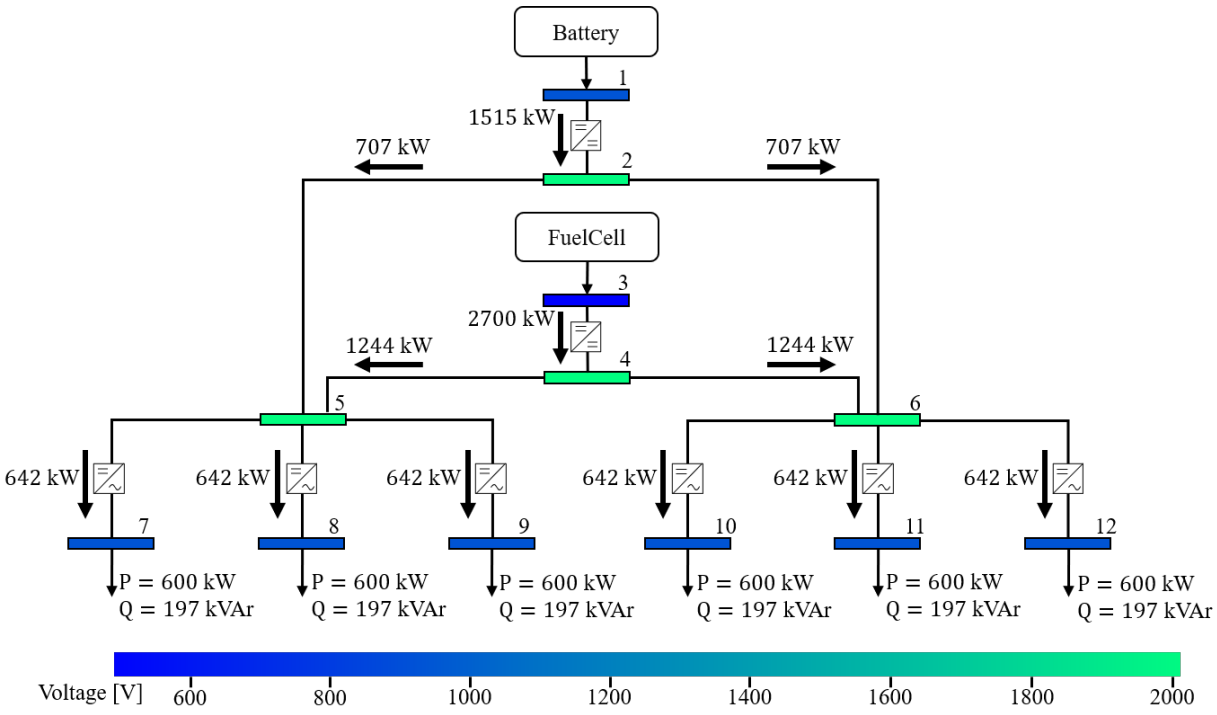

Figure 12: 12 bus regional aircraft powertrain during take-off

Because of the symmetric system definition, i.e. of the connection resistances, the power distribution is equal for the left and the right side of the powertrain. Overall a power loss of 615 kW occurs, which results in a powertrain efficiency of about 85 % in total, defined as output power divided by input or source power.
The bus voltage magnitudes are also represented in Figure 12 by the color of the buses. The voltage is set to 2 kV for the distribution at the buses 2, and 4 to 6. A defined voltage reduction is forced by the inverters to the buses 7 to 12, to meet the assumed motor voltage of $V_{rms}^{AC} = 1\,\text{kV}$.

DOI: 10.13009/EUCASS2023-475

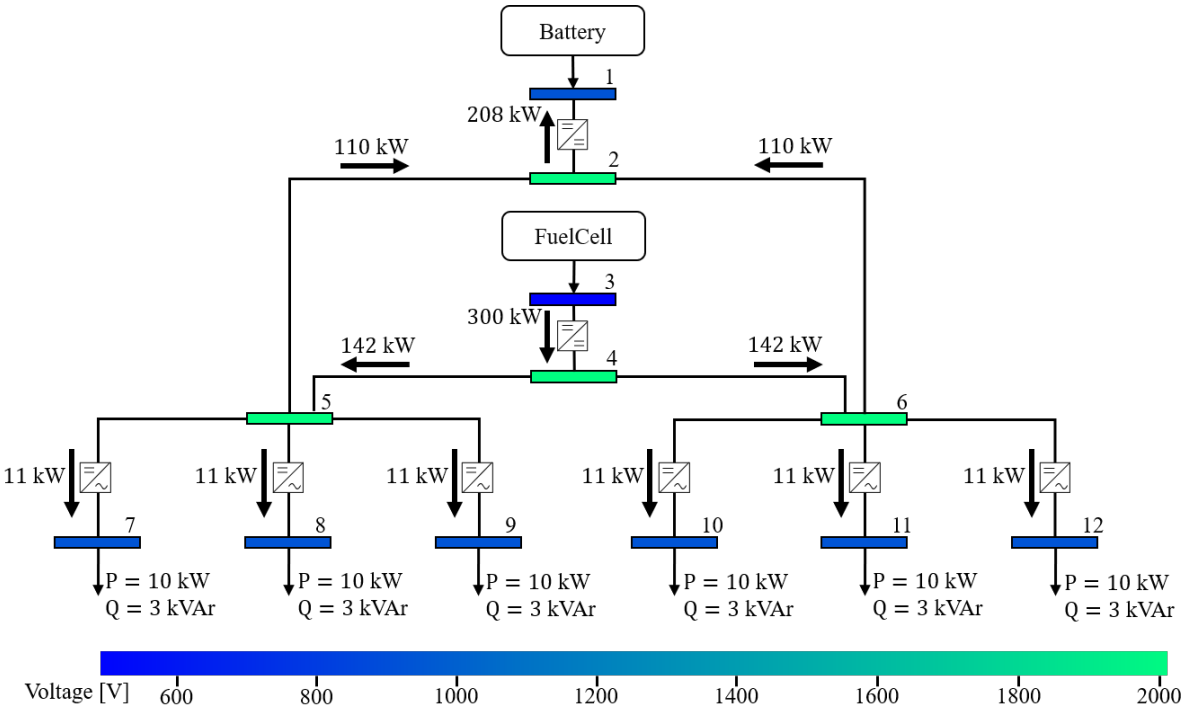

Figure 13: 12 bus regional aircraft powertrain during descent

The same distribution system, and therefore powertrain, is analysed for a different design point with a smaller power demand of the electric motors, representing a low-power flight phase such as the descent of the aircraft. Figure 13 illustrates the results for such an operating point with an active power demand of $P = 10\,\text{kW}$ per load. As mentioned before, the fuel cell has a minimum assumed power of 300 kW. However, the overall load power demand is less than the minimal fuel cell generator power. Hence, the fuel cell operates at its minimal power output and the battery is being charged. The power flow direction from bus 5 and 6 to bus 2, as well as the power flow direction from bus 2 to 1 is changed. Thereby, the battery gets charged with a total power of 208 kW. The power distribution ratio between both sides of the powertrain as well as the bus voltage levels are equal to the take-off case evaluated before. The operation of the converters and inverters with defined output voltages and variable modulation index allows the system to maintain the same bus voltage levels in different load cases. The total power loss in the system is 32 kW, while the overall efficiency is about 89 %. The efficiency is slightly increased compared to the high power demand operation point. Due to the reduced power flow at equal voltage levels, the resistive losses decreases and the efficiency increases.

4. Conclusion and Outlook

The present paper introduces a modified hybrid AC-DC load flow method to account for the challenges associated with power flow calculations of electrified powertrains suitable for aviation purposes. This method is suitable for all types of hybrid AC-DC systems including inverters, rectifiers, DC-DC and AC-AC converters. Thus, a vast variety of possible systems can be represented and solved as a whole with little computational cost. Using the proposed iteration logic, the method also allows for functional dependencies of system parameters.

The methodology and its implementation produce results, which are consistent with published data and the commercial software NEPLAN [18]. A maximum relative error of less than 0.02% was achieved. The widely applicable load flow method was used to analyse exemplary functional dependencies, such as converter efficiency. Furthermore, the methodology was successfully applied to simulate an electrified powertrain for a regional aircraft in two different flight phases.

Future work will focus on integration of realistic component models into the load flow analysis, such as for instance for electric motors or power electronics. With that it will be possible to size an electrified powertrain and analyse different off-design cases as well as a complete flight mission. The coupled component models and power flow calculations can furthermore be used for studies of partially electrified powertrains. Since the methodology can solve a closed electric system as a whole, it can also be integrated in performance calculations of hybrid electric powertrains including, for instance, a gas turbine and a generator.

DOI: 10.13009/EUCASS2023-475

References

[1] Europäische Kommission, Generaldirektion Mobilität und Verkehr, and Generaldirektion Forschung und Innovation. *Flightpath 2050 : Europe's vision for aviation : maintaining global leadership and serving society's needs*. Publications Office, 2011.

[2] David Wenzhong Gao, Chris Mi, and Ali Emadi. Modeling and simulation of electric and hybrid vehicles. *Proceedings of the IEEE*, 95(4):729–745, 2007.

[3] Noelle Janiaud, Francois-Xavier Vallet, Marc Petit, and Guillaume Sandou. Electric vehicle powertrain simulation to optimize battery and vehicle performances. In *2010 IEEE Vehicle Power and Propulsion Conference*, pages 1–5. IEEE, 2010.

[4] Manh-Kien Tran, Mobaderin Akinsanya, Satyam Panchal, and Roydon Fraser and Michael Fowler. Design of a hybrid electric vehicle powertrain for performance optimization considering various powertrain components and configurations.

[5] B. C. Raczkowski, M. Boyd, M. Johnson, R. Yeu, E. Walters, A. Donovan, and S. S. Patnaik. High-level integration sizing tool for electrical architectures (highlite). In *2022 IEEE Transportation Electrification Conference & Expo (ITEC)*, pages 225–230. IEEE, 2022.

[6] Seumas M. Beedie, Caleb M. Harris, Johannes A. Verberne, Cedric Y. Justin, and Dimitri Mavris. Modeling framework for identification and analysis of key metrics for trajectory energy management of electric aircraft. In *AIAA AVIATION 2021 FORUM*, VIRTUAL EVENT, 2021. American Institute of Aeronautics and Astronautics.

[7] Vincenzo Palladino, Arnaud Jordan, Nathalie Bartoli, Peter Schmollgruber, Valerie Pommier-Budinger, and Emmanuel Benard. Preliminary studies of a regional aircraft with hydrogen-based hybrid propulsion. In *AIAA AVIATION 2021 FORUM*, VIRTUAL EVENT, 2021. American Institute of Aeronautics and Astronautics.

[8] Francesco Orefice, Fabrizio Nicolosi, Salvatore Corcione, and Pierluigi Della Vecchia. Hybridization and mission analysis of a regional turboprop. In *AIAA AVIATION 2021 FORUM*, VIRTUAL EVENT, 2021. American Institute of Aeronautics and Astronautics.

[9] Mykhaylo Filipenko, Stefan Biser, Martin Boll, Matthias Corduan, Mathias Noe, and Peter Rostek. Comparative analysis and optimization of technical and weight parameters of turbo-electric propulsion systems. *Aerospace*, 7(8):107, 2020.

[10] B. Stott. Review of load-flow calculation methods. *Proceedings of the IEEE*, 62(7):916–929, 1974.

[11] Haytham M. A. Ahmed, Ayman B. Eltantawy, and M. M. A. Salama. A generalized approach to the load flow analysis of ac–dc hybrid distribution systems. *IEEE Transactions on Power Systems*, 33(2):2117–2127, 2018.

[12] Jingting Lei, Ting An, Zhengchun Du, and Zheng Yuan. A general unified ac/dc power flow algorithm with mtdc. *IEEE Transactions on Power Systems*, 32(4):2837–2846, 2017.

[13] Jef Beerten, Stijn Cole, and Ronnie Belmans. Generalized steady-state vsc mtdc model for sequential ac/dc power flow algorithms. *IEEE Transactions on Power Systems*, 27(2):821–829, 2012.

[14] Karl Friedrich Schäfer. Leistungsflussberechnung. In Karl Friedrich Schäfer, editor, *Netzberechnung*, pages 169–288. Springer Fachmedien Wiesbaden, Wiesbaden, 2020.

[15] Stefan Polster and Herwig Renner. *Berechnung elektrischer Energienetze*. TU Graz, Institute of Electrical Power Systems, 2017.

[16] Xi-Fan Wang, Yonghua Song, and Malcolm Irving. *Modern power systems analysis*. Power electronics and power systems. Springer, New York, NY, 2008.

[17] D. Krug, M. Malinowski, and S. Bernet. Design and comparison of medium voltage multi-level converters for industry applications. In *Conference Record of the 2004 IEEE Industry Applications Conference, 2004. 39th IAS Annual Meeting*, pages 781–790. IEEE, 3-7 Oct. 2004.

[18] PSI NEPLAN AG. https://www.neplan.ch/?lang=de.

[19] Jianjian Wang, Yuanyuan Sun, Yahui Li, Kejun Li, Jie Lou, Yonglian Liang, and Gonde Xu. *2020 IEEE/IAS Industrial and Commercial Power Systems Asia: (IEEE I&CPS Asia 2020) : July 13-16, 2020, Weihai, China*. IEEE, Piscataway, NJ, 2020.

DOI: 10.13009/EUCASS2023-475

Appendix

Table 9: System vectors and matrices for generalised load flow calculation

Symbol	Description	Value meaning
W	Boolean vector of bus type	0: AC bus, 1: DC bus
U	Boolean matrix of bus connection	0: buses not connected, 1: buses connected
D	Boolean matrix of line type	0: AC line, 1: DC line
C	Boolean matrix of converter existence between two buses	0: no converter, 1: converter in between
CAt	Boolean matrix if converter is defined at one particular bus	0: no converter, 1: converter placed

$$P_n^{inj} = \overline{W}_n \cdot \left(P_{G,n}^{AC} - P_{L,n}^{AC} + \eta_{n,I} P_{G,n}^{DC} - \frac{P_{L,n}^{DC}}{\eta_{n,R}}\right) + W_n \cdot \left(P_{G,n}^{DC} - P_{L,n}^{DC} + \eta_{n,R} P_{G,n}^{AC} - \frac{P_{L,n}^{AC}}{\eta_{n,I}}\right) \ , \ \forall n \in N \tag{32}$$

$$\begin{aligned} P_n^{cal} = \sum_{m=1}^{N} U_{nm} \cdot \Bigg[& \overline{W}_n \overline{W}_m \overline{D}_{nm} \overline{C}_{nm} \cdot \left(V_n^2 G_{nm} - V_n V_m \cdot (G_{nm} \cos(\theta_n - \theta_m) + B_{nm} \sin(\theta_n - \theta_m))\right) \\ & + \overline{W}_n \overline{W}_m \overline{D}_{nm} C_{nm} CAt_{nm} \cdot \left(V_n^2 t_{nm}^{-2} G_{nm} - V_n t_{nm}^{-1} V_m Y_{nm} \cos(\theta_n - \theta_m - \psi_{nm} + \theta_{C,nm})\right) \cdot \left(\frac{a_2}{\eta_{nm,1}} + b_2 \eta_{nm,2}\right) \\ & + \overline{W}_n \overline{W}_m \overline{D}_{nm} C_{nm} \overline{CAt}_{nm} \cdot \left(V_n^2 G_{nm} - V_n t_{nm}^{-1} V_m Y_{nm} \cdot \cos(\theta_n - \theta_m - \psi_{nm} - \theta_{C,nm})\right) \\ & + \overline{W}_n W_m D_{nm} \overline{C}_{nm} \cdot \left(G_{nm} \cdot (M_{nm}^{-2} V_n^2 - M_{nm}^{-1} V_n V_m)\right) \cdot \left(\frac{a_1}{\eta_{nm,R}} + b_1 \eta_{nm,I}\right) \\ & + W_n \overline{W}_m D_{nm} \overline{C}_{nm} \cdot \left(G_{nm} \cdot (V_n^2 - V_n M_{nm}^{-1} V_m)\right) \\ & + W_n W_m D_{nm} \overline{C}_{nm} \cdot \left(G_{nm} \cdot (V_n^2 - V_n V_m)\right) \\ & + W_n W_m D_{nm} C_{nm} CAt_{nm} \cdot \left(G_{nm} \cdot (V_n^2 t_{nm}^{-2} - V_n t_{nm}^{-1} V_m)\right) \cdot \left(\frac{a_2}{\eta_{nm,1}} + b_2 \eta_{nm,2}\right) \\ & + W_n W_m D_{nm} C_{nm} \overline{CAt}_{nm} \cdot \left(G_{nm} \cdot (V_n^2 - V_n t_{nm}^{-1} V_m)\right) \Bigg] \ , \ \forall n \in N \end{aligned} \tag{33}$$

$$Q_n^{inj} = \overline{W}_n \cdot (Q_{G,n}^{AC} - Q_{L,n}^{AC} + Q_{G,n}^{DC} - Q_{L,n}^{DC}) \ , \ \forall n \in N \tag{34}$$

$$\begin{aligned} Q_n^{cal} = \sum_{m=1}^{N} U_{nm} \cdot \Bigg[& \overline{W}_n \overline{W}_m \overline{D}_{nm} \overline{C}_{nm} \cdot \left(-V_n^2 B_{nm} - V_n V_m \cdot (G_{nm} \sin(\theta_n - \theta_m) - B_{nm} \cos(\theta_n - \theta_m))\right) \\ & + \overline{W}_n \overline{W}_m \overline{D}_{nm} C_{nm} CAt_{nm} \cdot \left(-V_n^2 t_{nm}^{-2} B_{nm} - V_n t_{nm}^{-1} V_m Y_{nm} \sin(\theta_n - \theta_m - \psi_{nm} + \theta_{C,nm})\right) \\ & + \overline{W}_n \overline{W}_m \overline{D}_{nm} C_{nm} \overline{CAt}_{nm} \cdot \left(-V_n^2 B_{nm} - V_n t_{nm}^{-1} V_m Y_{nm} \sin(\theta_n - \theta_m - \psi_{nm} - \theta_{C,nm})\right) \\ & + \overline{W}_n W_m D_{nm} \overline{C}_{nm} \cdot P_{nm}^{cal} \tan(\varphi_{nm}) \Bigg] \ , \ \forall n \in N \end{aligned} \tag{35}$$

with $\overline{C} = 1 - C$, $\overline{CAt} = 1 - CAt$, $\overline{D} = 1 - D$, $\overline{W} = 1 - W$ and a_1, b_1, a_2, b_2 from Equations (17) and (21).